scientific reports

Check for updates

OPEN

Prediction of the kinetic profiles in H-mode plasma discharges on EAST using core-pedestal coupling

Chaotong Yang[1], Kai Li[1]✉, Guoqiang Li[2], Yanjie Yang[2,3], Xiang Jian[2], Lin Yu[2,3], Tao Zhang[2], Qing Zang[2], Haiqing Liu[2], Xin Lin[2] & Jilei Hou[2]

The physical processes in tokamak plasma are strongly related to the coupling between the core and the pedestal. The accurate prediction of the kinetic profiles (electron temperature and density) from the pedestal to the core lays the physics basis for fusion performance optimization in future plasma-burning tokamak devices. Based on the optimized width model ($\Delta_\psi = 0.12\beta_{p,ped}^{1/2}$ between the pedestal width Δ_ψ and the square root of the poloidal pedestal beta $\beta_{p,ped}$) from empirical observations in type-I edge-localized mode (ELM) H-mode discharges, the REPED model is further used to predict the pedestal structures for type-III ELM H-modes on EAST in this work. By combining the REPED model and the TGYRO transport module, the core-pedestal coupling was initially employed for predicting the kinetic profiles ranging from the axis to the separatrix in H-mode plasma discharges on EAST.

Keywords EAST, Core-pedestal coupling, Kinetic profile, Pedestal structure, REPED model

The interaction between the pedestal and the core in tokamak plasma is considered important in understanding the high-confinement mode (H-mode) plasma discharge behaviour[1–4]. It was relatively early found that the peeling–ballooning (PB) stability in tokamak plasma can be affected by the global Shafranov shift[5], where the PB stability is determined by the pressure gradient and current profiles. In the widely-used EPED model[4–6], the pedestal structure is determined using the two constraints: the PB mode (PBM) and the kinetic ballooning mode (KBM) in H-mode plasma discharges; PBM and KBM strongly affect the core pressure (or core confinement). Additionally, the core confinement and turbulent transport depend on (a) the plasma equilibrium, (b) the density and temperature profiles and (c) the heating and particle sources. Therefore, the core-pedestal transport process must be studied to better understand the interaction between the H-mode pedestal and the core in tokamak plasma.

An integrated modeling workflow was developed to predict the kinetic profiles ranging from the axis to the separatrix for DIII-D discharges[1], which mainly based on the EPED model and the TGYRO transport module[7], and the workflow shown the predictions were a good agreement with experiments. A similar workflow has also been employed in steady-state scenarios implemented in the China Fusion Engineering Test Reactor (CFETR)[8]. The Experimental Advanced Superconducting Tokamak (EAST) is a fully superconducting tokamak device, which has achieved a series of records in steady-state long-pulse H-mode operation in past experimental campaigns[9–11]. Studies on the H-mode transport simulation using integrated modeling on EAST have been reported[12]; however, in these studies, a fixed pedestal profile (fixed electron density and temperature) was obtained from experiments[9] when using the TGYRO transport module. Meanwhile, the pedestal simulations primarily focused on the kinetic profiles in the edge region and employed a simple function to represent the core profile on EAST[13], which this approach often neglects the peak conditions of core plasma. Conversely, certain diagnostic systems may not offer real-time data or are susceptible to considerable measurement errors during experiments. Therefore, the ability to swiftly deliver kinetic profiles for H-mode discharges on EAST through the application of core-pedestal coupling is of particular significance.

In this paper, the core-pedestal coupling is employed to predict the kinetic profiles ranging from the axis to the separatrix for EAST H-mode plasmas, which is based on the REPED model[13] and the TGYRO transport module. The REPED model was successfully applied to the prediction of the pedestal height in type-I edge-localized mode (ELM) in H-mode discharges on EAST[13], where the width model ($\Delta_\psi = 0.12\beta_{p,ped}^{1/2}$, Δ_ψ is

[1]Centre for Theoretical and Computational Physics, College of Physics, Qingdao University, Qingdao 266071, China. [2]Institute of Plasma Physics, Hefei Institutes of Physical Science, Chinese Academy of Sciences, Hefei 230031, China. [3]University of Science and Technology of China, Hefei 230026, China. ✉email: kaili@qdu.edu.cn

Plasma parameters					
Shot	102187	80678	69033	54863	54845
Time (ms)	7700	4910	3950	3650	3450
Plasma current I_p (kA)	450	415	460	460	460
Line-average density $\langle n_e \rangle$ (10^{19} m^{-3})	5.33	3.78	5.64	5.47	3.84
Plasma Stored energy W (MJ)	1.73	1.26	1.55	1.40	1.43
Normalized toroidal beta β_N	1.14	1.31	0.91	1.19	1.21
Poloidal beta β_p	1.15	0.98	0.99	0.91	0.92
Toroidal magnetic field B_T (T)	2.43	1.63	2.48	1.67	1.68
Power of NBI P_{NBI} (MW)	2.6	2.2	6.2	2.5	2.4
Power of LHW P_{LHW} (MW)	1.8	0.8	3.0	1.2	2.0

Table 1. The plasma major parameters for type-III ELMs H-mode discharges.

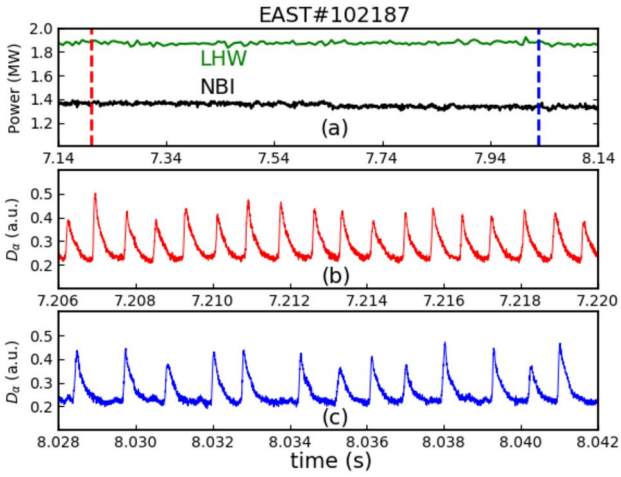

Fig. 1. The heating power and D_α are plotted for two time slices (7.2 s and 8.03 s).

the pedestal width and $\beta_{p,ped}$ is the poloidal pedestal beta) was optimized based on experimental observations; compared to the EPED model[4], the coefficient between Δ_ψ and $\beta_{p,ped}^{1/2}$ in EAST (~ 0.12) is higher than that in DIII-D (~ 0.076). Despite the type-III ELMs could be driven by the resistive ballooning instabilities from previous analysis in EAST[14,15], the REPED model may still predict the pedestal height, and then we further explore the applicability of the optimized width model in type-III ELM H-modes from EAST experiments. For the core plasma, the prediction of the kinetic profiles (electron density and temperature) was successfully achieved using the TGYRO transport solver[12,16].

The paper is organized as follows. In "Validation of the REPED model against type-III ELMs in H-mode plasma discharges on EAST" section, the REPED model is validated against the type-III ELMs in H-mode plasma discharges on EAST. In "Application of core-pedestal coupling with self-consistent pedestal structure in EAST simulation" section, an application of the core-pedestal coupling with a self-consistent pedestal structure is described for the EAST simulation, and the prediction of the kinetic profiles is compared with experiments for H-mode discharges. Finally, a discussion and a summary are presented in "Summary and discussion" section.

Validation of the REPED model against type-III ELMs in H-mode plasma discharges on EAST

To perform the core-pedestal coupling simulation, it is necessary to investigate the applicability and reliability of the REPED model in H-mode discharges on EAST. The REPED model has been used to calculate the pedestal height for type-I ELMs in H-mode discharges based on the optimized width model. We will investigate the suitability of the REPED model in the prediction of type-III ELMs in H-mode plasma discharges. During the past years, several experiments on type-III ELMs in H-mode discharges were conducted to better understand the ELM behaviour and control[14,15,17,18]. In this study, these experimental results will be used to validate the prediction of type-III ELMs in H-mode plasma discharges. Table 1 lists the main global plasma parameter values used in the selected discharges; these values have provided a good coverage of the type-III ELM H-mode discharges.

The ELM is categorized to be type-III due to its inverse correction between ELM frequency and the heating power for discharge 102187, which is shown in Fig. 1, the red and blue represent the higher heating power and

lower heating power, respectively. In addition, Fig. 2 shows that the poloidal beta and the pedestal electron collisionality are calculated for the selected discharges in Table 1, and consist with the type-III ELM regime in JET and JT-60U[19], which is another evidence that those discharges are type-III ELMs on EAST.

The following diagnostics were used to obtain the experimental density and temperature profiles: (1) The electron density n_e profiles were measured by the Thomson scattering (TS) diagnostic[20] and the density profile reflectometry (DPR)[21]; then the line-integrated density of the fitted n_e profiles was compared with the measurements obtained using the 11-channel POlarimeter-INTerferometer (POINT) diagnostic system[22]. The electron temperature T_e profiles were also measured by TS diagnostic. (2) The Charge eXchange Recombination Spectroscopy (CXRS) provided the core ion temperature T_i profile[23]; based on the experimental observation that T_i and T_e are similar at the pedestal top, we set $T_i = T_e$ in the collisional pedestal region. (3) The effective charge number Z_{eff} was obtained from visible bremsstrahlung measurements[24].

Based on the experimental profiles, the pressure pedestal structure was calculated using kinetic equilibrium reconstruction[25] for type-III ELMs in H-mode discharges, and the pedestal width Δ_ψ (normalized poloidal flux ψ space) and pedestal height p_{ped} were obtained using the modified hyperbolic tangent (mtanh) function[26]. The detailed calculation procedure has been described in[13].

The REPED model is an implementation of the EPED model; the main difference is that in the REPED model, the equilibrium calculation is performed using the TEQ equilibrium solver based on the Corsica code[27], whereas in the EPED model, the equilibrium calculation is based on the TOQ code. The TEQ code is that it allows to conveniently construct equilibrium for general geometry while TOQ code only applies to up-down symmetric geometry, such an advantage can be important in the pedestal region. The predicted pedestal structures were determined by the two constraints of PBM and the width model in the REPED model. In the width model, the scaling $\Delta_\psi = 0.12\beta_{p,ped}^{1/2}$ between the pedestal width Δ_ψ and the square root of the poloidal pedestal beta $\beta_{p,ped}$ was obtained from experimental observations on EAST, which is plotted in Fig. 3; the circle points are type-III ELMs and also shows that the pedestal width correlated with $\beta_{p,ped}$, thus the scaling was also used in REPED model for type-III ELMs H-mode discharges. The PBM stability boundary was calculated using the ELITE code[28–30]. Initially, the TEQ equilibrium solver was used to construct a set of equilibria with various pedestal widths and heights, which were used to run the ELITE code. To construct these equilibria, the pressure and current (or safety factor) profiles are required. The pressure profile was calculated using formula $p = n_e T_e + (n_i + n_z)\, T_i$, where $T_i = T_e$ in this model; the ion density n_i and impurity density n_z were calculated by quasi-neutrality and Z_{eff}, with Z_{eff} obtained from experiments and is assumed to be constant across the whole minor radius. The Z_{eff} is considered in both the pedestal modeling through effecting the bootstrap current, and the core transport modeling though dilution effect. The n_e and T_e profiles are set up from the pedestal to core by the following analytical formulas[31,32]:

$$n_e(\psi) = n_{sep} + a_{n0}\left\{\tanh\left[\frac{2(1-\psi_{mid})}{\Delta_\psi}\right] - \tanh\left[\frac{2(\psi-\psi_{mid})}{\Delta_\psi}\right]\right\} + a_{n1}\mathrm{H}\left(1-\frac{\psi}{\psi_{ped}}\right)\left[1-\left(\frac{\psi}{\psi_{ped}}\right)^{\alpha_{n1}}\right]^{\alpha_{n2}} \quad (1)$$

$$T_e(\psi) = T_{sep} + a_{T0}\left\{\tanh\left[\frac{2(1-\psi_{mid})}{\Delta_\psi}\right] - \tanh\left[\frac{2(\psi-\psi_{mid})}{\Delta_\psi}\right]\right\} + a_{T1}\mathrm{H}\left(1-\frac{\psi}{\psi_{ped}}\right)\left[1-\left(\frac{\psi}{\psi_{ped}}\right)^{\alpha_{T1}}\right]^{\alpha_{T2}} \quad (2)$$

where Δ_ψ is the pedestal width in ψ space, $\psi_{mid} = 1 - \Delta_\psi/2$, and $\psi_{ped} = 1 - \Delta_\psi$; H is the Heaviside step function, and tanh is the hyperbolic tangent function. In formulas (1) and (2), we set the following parameter values: $n_{sep} = n_{e,ped}/4$, $T_{sep} = 50$eV, $a_{n0} = 1.0$, $\alpha_{n1} = 0.9$, $\alpha_{n2} = 1.8$, $\alpha_{T1} = 1.2$ and $\alpha_{T2} = 1.4$ in the EAST simulation. The n_e profile was constrained by $\langle n_e \rangle$ and the density peaking factor, a_{T1} was adjusted to

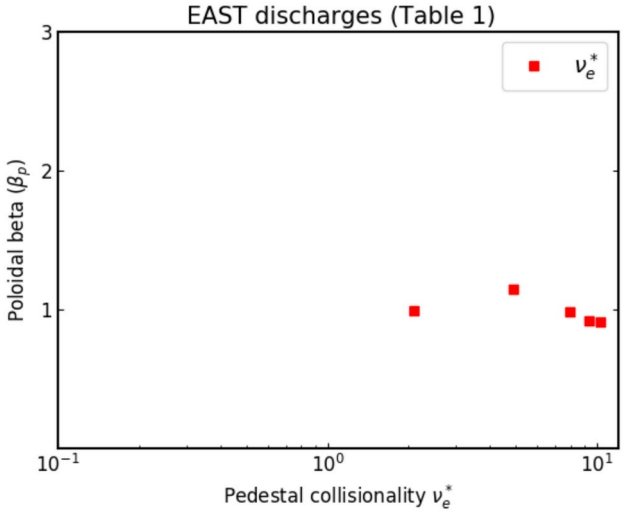

Fig. 2. The comparison of the poloidal beta and the pedestal electron collisionality for the selected discharges in Table 1.

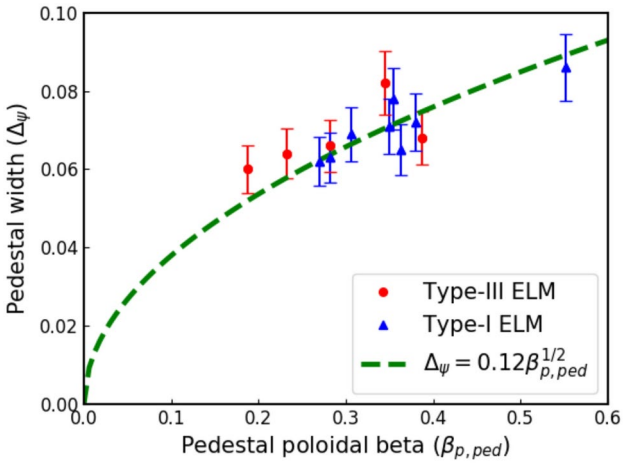

Fig. 3. The measurements of Δ_ψ and $\beta_{p,ped}$ are plotted for type-III and type-I ELMy H-mode discharges on EAST.

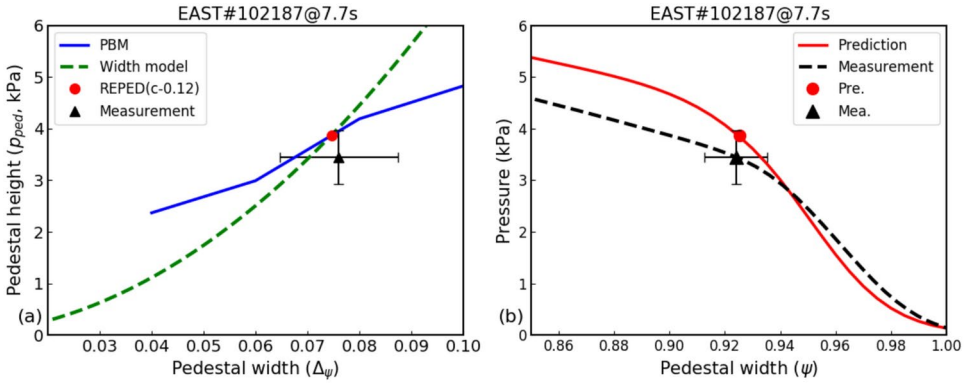

Fig. 4. (**a**) An illustration of the REPED model and (**b**) the predicted and measured pressure profiles in the pedestal region for type-III ELM H-mode plasmas. Input parameters of the model correspond to discharge 102187. The red circle represents the prediction and the black triangle is the measurement with 15% error bar.

maintain β_N for the T_e profiles; then, profiles with various pedestal heights and widths were set by scanning the two free coefficients Δ_ψ and a_{T0}. Next, the current density profile in the pedestal was calculated using the Sauter bootstrap current model[33,34]; the core current profile is a simple function, which was scaled to match the total current. Finally, the set of equilibria was generated with various pedestal widths and heights by scanning a_{T0} for each pedestal width ($\Delta_\psi = 0.04, 0.06, 0.07, 0.08, 0.1$). Based on these equilibria, the ELITE code was used to calculate the PBM stability for a wide range of mode numbers (typically $n = 5 - 30$); then, the critical pedestal height values were calculated for each Δ_ψ. The PBM stability boundary was composed of these critical values.

Figure 4 shows a comparison of the measured and predicted pedestal structures for the type-III ELMs in H-mode discharges. The blue solid line represents the PBM stability boundary obtained using the ELITE code in Fig. 4a, and the green dashed line represents the width model; the red intersection of the two lines provides the predicted pedestal width and height based on the REPED model, and the measured value is indicated by the black point. The estimated measurement error is 15%[35]. The pedestal pressure profiles are also plotted for prediction and measurement in Fig. 4b. In Fig. 4, the predicted pedestal structure is close to the experimentally obtained structure, demonstrating the ability of the REPED model to predict the pedestal structure for type-III ELMs in H-mode discharges on EAST.

Furthermore, we compared the REPED model predictions with measurements for other type-III ELMs discharges; the pedestal heights are plotted in Fig. 5. The horizontal and vertical coordinates represent the predicted pedestal heights and the measured heights, respectively; the diagonal line shows a perfect agreement. In summary, Fig. 5 indicates that the REPED model can be used to predict the pedestal structure for type-I and type-III ELMs in H-mode discharges on EAST.

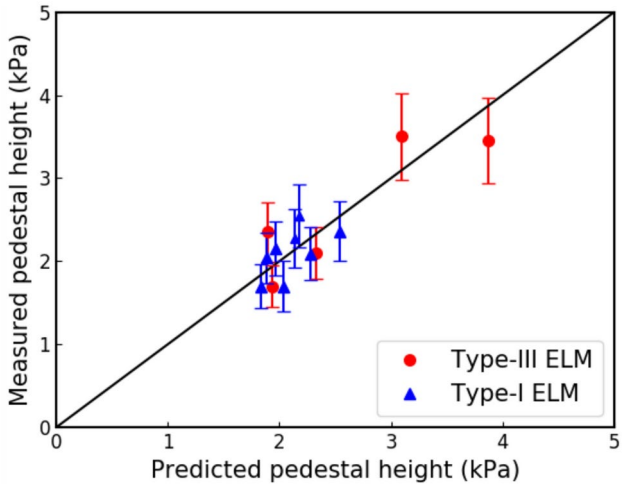

Fig. 5. A comparison of the predictions to measured pedestal height for H-mode plasma discharges on EAST. The red points are the pedestal heights of type-III ELM discharges and the blue triangles represent the type-I ELM H-modes.

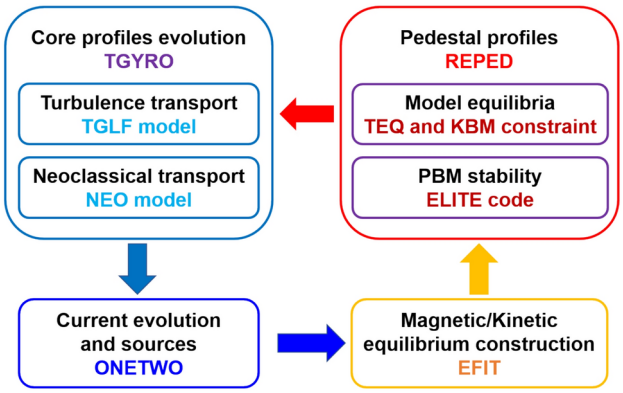

Fig. 6. An illustration of core-pedestal coupling for EAST H-mode simulation. The pedestal profiles are provided by the REPED model and TEQ equilibrium solver. The ONETWO code calculates the sources of particles and heat based on the predicted profiles with self-consistent pedestal structure. The core profiles are predicted by the TGYRO module and the EFIT code constructs the magnetic/kinetic equilibria.

Application of core-pedestal coupling with self-consistent pedestal structure in EAST simulation

The core-pedestal coupling with self-consistent pedestal structure

In "Validation of the REPED model against type-III ELMs in H-mode plasma discharges on EAST" section, the REPED model was used to predict the pedestal height for type-I and type-III ELMs in H-mode plasma discharges on EAST. The integrated modeling workflow[1] in the One Modeling Framework for Integrated Tasks (OMFIT)[36,37] has been used to study the core transport iterative analysis and predict the kinetic profiles in current[1,8,38] and future tokamak devices[8,12]. Here, we replace the EPED model in the integrated modeling with the REPED model and conveniently perform core-pedestal coupling simulation for EAST H-mode discharges.

Figure 6 shows the core-pedestal coupling simulation process for the pedestal structure, core profiles and kinetic equilibrium. The inputs to the initial iteration were obtained the magnetic EFIT equilibrium[39] shown in Fig. 6. Then, the profiles with the pedestal structure were obtained using the REPED model. The ONETWO transport code[40,41] was used to calculate the sources and sinks of the energy and particle in the plasma, where the lower hybrid wave (LHW) was evaluated using the ray-tracing code GENRAY[42] and the Fokker–Planck Code CQL3D[43]. By calling multiple instances of the theory-based turbulent transport code TGLF[44] and neoclassical transport code NEO[45], TGYRO was used to obtain the transport fluxes of particles and energy and to calculate the steady-state profiles of density and temperature. The saturation rule (TGLF-SAT1)[9] was employed in this paper. The following is a new run of the REPED model with the updated global plasma parameter values. The next cycle is repeated until the T_e evolution no longer varies (or the electron flux reaches the target flux). Furthermore, we reconstructed the kinetic equilibrium with the predicted profiles using the EFIT code again.

Comparison of profile predictions with experiments in H-mode plasma discharges

Using the main plasma parameters in H-mode discharges, we predicted the kinetic profiles ranging from the axis to the separatrix using core-pedestal coupling and compared the predictions with experiments for H-mode discharges.

In this section, we predicted the kinetic profiles of the type-I ELM (56924) and type-III ELM (102187) H-mode. The prediction process includes the following main steps:

1. Run EFIT to obtain the equilibrium and main parameters from experimental data at an initial time t_0. Then, the REPED model was used to predict the pressure pedestal structures, and the TEQ code constructed the initial kinetic profiles (n_e and T_e, $T_i = T_e$) based on the predicted pedestal.
2. The initial kinetic profiles were inserted into the GENRAY with CQL-3D for the LHW calculation; then, the ONETWO transport code calculated the sources and sinks of energy and particles.
3. The equilibrium and sources were used as inputs to the TGYRO code, and the T_e and T_i evolutions were initially calculated keeping n_e fixed; next, the n_e evolution was calculated keeping the temperatures basically unchanged. Finally, the TGYRO code provided the kinetic profiles in the core region ($\rho = 0.2 - 0.8$).
4. The EFIT code was employed again to update the equilibrium based on the predicted kinetic profiles, which were used for a new run of the REPED model.
5. The process from step (2) to step (4) was repeated until the profiles remained unchanged with the increase in number of iteration times.

Figure 7 shows the predicted electron density and temperature obtained using the core-pedestal coupling for EAST discharge 56924. The black circles and lines represent the experimental profiles of electron density n_e (Fig. 7a) and electron temperature T_e (Fig. 7b) in normalized ρ, and the red solid lines represent the predicted kinetic profiles. A good agreement between predictions and measurements is observed, as indicated by the red lines representing the measurement error for the type-I ELM H-modes on EAST.

Although the predicted n_e and T_e are close to the measurements, the ion temperature T_i is not compared here because of the lack of diagnostic data for the discharge 56924. Thus, we employed relatively complete diagnostic data of the discharge 102187 to compare the T_i profiles, as shown in Fig. 8. The black circles and lines represent the experimental profiles of n_e (Fig. 8a), T_e (Fig. 8b) and T_i (Fig. 8c) in normalized ρ; the red solid lines represent the predicted kinetic profiles. The predicted T_e and T_i are very close to the measurements; however, the predicted n_e profile is lower than the measured profile in the core region. The discharge 102187 was carried out with argon (Ar) seeding for better studying the large ELM control on EAST[15], and it is worth pointing out that the effects on the pedestal with impurity seeding (N_2, Ne, Ar, Kr, etc.) has been widely observed in many devices[46–49]. In this study, the increased core n_e after Ar seeding is speculated to be caused by the Ar impurity ionization, the change of ELM-induced particle flux and the disappearance of the pedestal edge coherent mode (ECM) fluctuation. The reason that the simulated and experimental kinetic profiles do not perfectly match might be induced by diagnostic limitation, for example, only the volume averaged Z_{eff} value can be obtained in experiments, we assume the Z_{eff} value to be flat in modeling but should have a radial variation under experiments, which can have some effect on the background turbulence.

By comparing the experiments with the simulations, we initially predicted the density and temperature profiles ranging from the axis to the separatrix with the core-pedestal-coupled simulation for EAST H-mode discharges. Although the predicted T_e and T_i are in good agreement with the measurements, the predicted core n_e profile is lower than the experimental profile for discharge 102187; thus, we need to consider the discharge conditions in the H-mode simulations on EAST.

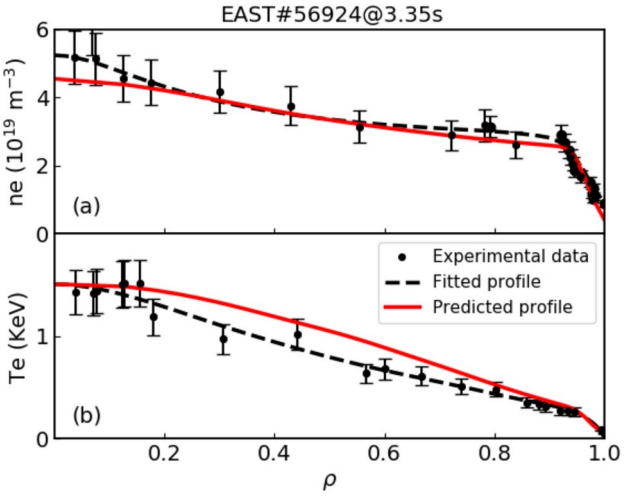

Fig. 7. The measured and predicted profiles of (**a**) n_e and (**b**) T_e for EAST discharge 56924. The black circles and triangles are experimental data and the red lines represent the predicted kinetic profiles.

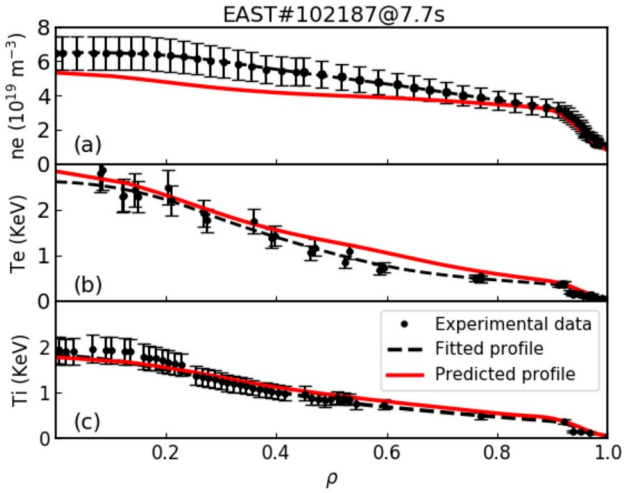

Fig. 8. The comparison of profile predictions with experiments are plotted for EAST discharge 102187. The circles and triangles are raw data with 15% measurement error, the black dashed lines are the fitted profiles, and the red solid lines represent the predicted kinetic profiles.

Summary and discussion

In this study, we investigated the application of core-pedestal coupling for predicting the kinetic profiles in H-mode discharges on EAST. Additionally, we demonstrated that the REPED model and the TYGRO transport module can provided initial predictions of the kinetic profiles ranging form the core to the pedestal through a series of comparisons between experiments and simulations.

In the core-pedestal coupling simulation, the TGYRO transport module and the REPED model serve as simulation cornerstones; the TGYRO module was extensively used to predict the profiles in the core region. This work validated the applicability of the REPED model by predicting the pedestal structures for type-III ELMs in H-mode discharges on EAST. We understand that type-III ELMs should be described by resistive MHD, here we apply ideal MHD constraints to test to which extent that the ideal MHD, which is more convenient and faster in practice use, can predict the pedestal structure of the type-III ELMs using the REPED model. However, the caveat is that the conclusion drawn here might not be general and more discharges should be tested in the future. Finally, a comparison between predictions and measurements for EAST H-mode discharges, showed the predicted T_e and T_i profiles are in good agreement with experimental measurements; differences were observed in the core n_e profile because of the H-mode discharge with the impurity seeding. The core-pedestal coupling is validated for the first time in EAST H-mode discharges, which has the potential to rapidly provide the kinetic profiles in real-time experiments for other physical research purposes.

However, several issues require further investigation. For example, this study was based on a limited number of type-III ELMs in H-mode discharges; therefore, it is essential to construct a larger pedestal database to improve the reliability of the REPED model on EAST. Regarding the discharge 102187, the simulated core electron density is lower than the measured density. This differences were observed in the core n_e profile because of the H-mode discharge with the impurity seeding. While there indeed exists some discrepancies between the experiments and simulation kinetic profiles, the overall agreement is acceptable. The difference might come from the diagnostic uncertainties like the q profile or rotation profiles et al. In addition, it is noted that the Z_{eff} profile, which we assume to be flat in the core region due to the lack of radial measurement, should have a radial variation which can have a remarkable effect on the background turbulence. A detailed systematic study in the validation of the transport model should be done in a future study. Additionally, our objective is to refine the core-pedestal coupling simulation to improve its generality and adaptability. Furthermore, it is worthwhile to predict the kinetic profiles under different discharge conditions; this would be useful in core-pedestal transport research and fusion performance optimization (Supplementary Information).

Data availability

The datasets used and analysed during the current study available from the corresponding author on reasonable request.

Received: 24 November 2024; Accepted: 10 March 2025
Published online: 17 March 2025

References

1. Meneghini, O. et al. Integrated fusion simulation with self-consistent core-pedestal coupling. *Phys. Plasmas.* **23**, 042507 (2016).
2. Kinsey, J. et al. Burning plasma projections using drift-wave transport models and scalings for the H-mode pedestal. *Nucl. Fusion.* **43**, 1845 (2003).

3. Snyder, P. B. et al. Stability and dynamics of the edge pedestal in the low collisionality regime: physics mechanisms for steady-state ELM-free operation. *Nucl. Fusion.* **47**, 961 (2007).
4. Snyder, P. B. et al. Development and validation of a predictive model for the pedestal height. *Phys. Plasmas.* **16**, 056118 (2009).
5. Urano, H. et al. Pedestal structure in H-mode plasmas. *Nucl. Fusion.* **54**, 116001 (2014).
6. Snyder, P. B. et al. A first-principles predictive model of the pedestal height and width: development, testing and ITER optimization with the EPED model. *Nucl. Fusion.* **51**, 103016 (2011).
7. Candy, J. et al. Tokamak profile prediction using direct gyrokinetic and neoclassical simulation. *Phys. Plasmas.* **16**, 060704 (2009).
8. Chen, J. L. et al. Self-consistent modeling of CFETR baseline scenarios for steady-state operation. *Plasma Phys. Control. Fusion.* **59**, 075005 (2017).
9. Wu, M. Q. et al. Transport simulation of EAST long-pulse H-mode discharge with integrated modeling. *Nucl. Fusion.* **58**, 046001 (2018).
10. Huang, J. et al. Long-pulse high-performance H-mode plasmas achieved on EAST. *Phys. Plasmas.* **30**, 062504 (2023).
11. Gong, X. Z. et al. Overview of recent experimental results on the EAST tokamak. *Nucl. Fusion.* Accepted Manuscript online (2024).
12. Gong, X. Z. et al. EAST steady-state long pulse H-mode with core-edge integration for CFETR. *Nucl. Fusion.* **62**, 076009 (2022).
13. Li, K. et al. Study of H-mode pedestal predictive model on EAST tokamak. *Plasma Phys. Control. Fusion.* **62**, 115007 (2020).
14. Lin, X. et al. Physical mechanisms for the transition from type-III to large ELMs induced by impurity injection on EAST. *Phys. Lett. A.* **431**, 127988 (2022).
15. Li, K. D. et al. Compatibility of large ELM control and stable partial detachment with neon/argon seeding in EAST. *Nucl. Fusion.* **63**, 026025 (2023).
16. Kinsey, J. et al. ITER predictions using the GYRO verified and experimentally validated trapped gyro-Landau fluid transport model. *Nucl. Fusion.* **51**, 083001 (2011).
17. Hou, J. L. et al. Deuterium pellet fueling in type-III ELMy H-mode plasmas on EAST superconducting tokamak. *Fusion Eng. Des.* **145**, 79–86 (2019).
18. Chen, S. D. et al. Parametric dependence of type-I and type-III ELMS and dynamic characteristics for ELM filaments in EAST tokamak. *IEEE Trans. Plasma Sci.* **47**, 799–806 (2018).
19. Oyama, N. et al. Pedestal conditions for small ELM regimes in tokamaks. *Plasma Phys. Control. Fusion.* **48**, A171 (2006).
20. Zang, Q. et al. The circuit of polychromator for Experimental Advanced Superconducting Tokamak edge Thomson scattering diagnostic. *Rev. Sci. Instrum.* **84**, 093504 (2013).
21. Zhang, S. B. et al. Density profile and fluctuation measurements by microwave reflectometry on EAST. *Plasma Sci. Technol.* **16**, 311 (2014).
22. Liu, H. Q. et al. Initial measurements of plasma current and electron density profiles using a polarimeter/interferometer (POINT) for long pulse operation in EAST. *Rev. Sci. Instrum.* **87**, 11D903 (2016).
23. Li, Y. Y. et al. First measurement of the edge charge exchange recombination spectroscopy on EAST tokamak. *Rev. Sci. Instrum.* **87**, 11E501 (2016).
24. Chen, Y. J. et al. Measurement and analysis of Zeff in EAST tokamak. *Plasma Phys. Control. Fusion.* **56**, 105006 (2014).
25. Li, G. Q. et al. Kinetic equilibrium reconstruction on EAST tokamak. *Plasma Phys. Control. Fusion.* **55**, 125008 (2013).
26. Groebner, R. J. et al. Progress in quantifying the edge physics of the H mode regime in DIII-D. *Nucl. Fusion* **41**, 1789 (2001).
27. Crotinger, J. A., LoDestro, L., Pearlstein, L. D., Tarditi, A., Casper, T. A. and Hooper, E. B. Corsica: a comprehensive simulation of toroidal magnetic-fusion devices. *Final report to the LDRD Program* (No. UCRL-ID-126284) (1997).
28. Wilson, H. R. et al. Ideal magnetohydrodynamic stability of the tokamak high-confinement-mode edge region. *Phys. Plasmas* **6**, 1925 (1999).
29. Wilson, H. R. et al. Numerical studies of edge localized instabilities in tokamaks. *Phys. Plasmas.* **9**, 1277 (2002).
30. Snyder, P. B. et al. Edge localized modes and the pedestal: a model based on coupled peeling–ballooning modes. *Phys. Plasmas* **9**, 2037 (2002).
31. Connor, J. W. et al. Magnetohydrodynamic stability of tokamak edge plasmas. *Phys. Plasmas* **5**, 2687 (1998).
32. Snyder, P. B. & Wilson, H. R. Ideal magnetohydrodynamic constraints on the pedestal temperature in tokamaks. *Plasma Phys. Control Fusion* **45**, 1671 (2003).
33. Sauter, O., Angioni, C. & Lin-Liu, Y. R. Neoclassical conductivity and bootstrap current formulas for general axisymmetric equilibria and arbitrary collisionality regime. *Phys. Plasmas.* **6**, 2834 (1999).
34. Sauter, O., Angioni, C. & Lin-Liu, Y. R. Neoclassical conductivity and bootstrap current formulas for general axisymmetric equilibria and arbitrary collisionality regime. *Phys. Plasmas.* **9**, 5140 (2002).
35. Zang, Q. et al. Characteristics of edge pedestals in LHW and NBI heated H-mode plasmas on EAST. *Nucl. Fusion.* **56**, 106003 (2016).
36. Meneghini, O. et al. Integrated modeling of tokamak experiments with OMFIT. *Plasma Fusion Res.* **8**, 2403009 (2013).
37. Meneghini, O. et al. Integrated modeling applications for tokamak experiments with OMFIT. *Nucl. Fusion.* **55**, 083008 (2015).
38. Zhai, X. M. et al. Validation of theory-based integrated modeling and new insights for a high-performance steady-state scenario with only RF heating on EAST. *Nucl. Fusion.* **62**, 076015 (2022).
39. Lao, L. L. et al. Reconstruction of current profile parameters and plasma shapes in tokamaks. *Nucl. Fusion* **25**, 1611 (1985).
40. Pfeiffer, W. W. et al. *ONETWO: A Computer Code for Modeling Plasma Transport in Tokamaks*. Medium: X; Size: Pages: 201 (General Atomic Co., 1980).
41. St John, H. et al. Transport simulation of negative magnetic shear discharges. In *15th Int. Conf. on Plasma Physics and Controlled Nuclear Fusion Research*, 603 https://doi.org/10.2172/10104519) (IAEA, 1994).
42. Smirnov, A. et al. Bull Amer. Phys. Soc. **39,** 1626 http://compxco.com/Genray_manual.pdf (1994).
43. Harvey, R. W. & McCoy, M. G. The CQL3D Code Proc. *IAEA TCM on Advances in Sim. and Modeling of Thermonuclear Plasmas* (ed.) 489–526 (1992).
44. Staebler, G., Kinsey, J. & Waltz, R. A theory-based transport model with comprehensive physics. *Phys. Plasmas.* **14**, 055909 (2007).
45. Belli, E. & Candy, J. An Eulerian method for the solution of the multi-species drift-kinetic equation. *Plasma Phys. Control. Fusion.* **51**, 075018 (2009).
46. Glöggler, S. et al. Characterisation of highly radiating neon seeded plasmas in JET-ILW. *Nucl. Fusion.* **59**, 126031 (2019).
47. Kallenbach, A. et al. Impurity seeding for tokamak power exhaust: from present devices via ITER to DEMO. *Plasma Phys. Control. Fusion.* **55**, 124041 (2013).
48. Eldon, D. et al. An analysis of controlled detachment by seeding various impurity species in high performance scenarios on DIII-D and EAST. *Nucl. Mater. Energy.* **27**, 100963 (2021).
49. Xue, G. Q. et al. Enhancement of plasma ion temperature by impurity seeding in H-mode plasmas. *Nucl. Fusion.* **61**, 116048 (2021).

Acknowledgements

This work was supported by the National Natural Science Foundation of China under Grant No. 12205157. The authors would like to acknowledge the ShenMa High Performance Computing Cluster at the Institute of Plasma Physics, Chinese Academy of Sciences. The authors thank Dr. Philip for providing the ELITE code, and also thank Dr. Lynda LoDestro at LLNL for providing the CORSICA code.

Author contributions

Chaotong Yang and Kai Li wrote the main manuscript text, Guoqiang Li, Yanjie Yang and Xiang Jian reviewed the manuscript, Lin Yu, Tao Zhang, Qing Zang, Haiqing Liu, Xin Lin, and Jilei Hou provided the experimental data.

Declarations

Competing interests

The authors declare no competing interests.

Additional information

Supplementary Information The online version contains supplementary material available at https://doi.org/10.1038/s41598-025-93919-0.

Correspondence and requests for materials should be addressed to K.L.

Reprints and permissions information is available at www.nature.com/reprints.

Publisher's note Springer Nature remains neutral with regard to jurisdictional claims in published maps and institutional affiliations.